Science Advances

AAAS

advances.sciencemag.org/cgi/content/full/3/3/e1601858/DC1

Supplementary Materials for

Explaining recurring maser flares in the ISM through large-scale entangled quantum mechanical states

Fereshteh Rajabi and Martin Houde

Published 24 March 2017, *Sci. Adv.* **3**, e1601858 (2017)
DOI: 10.1126/sciadv.1601858

This PDF file includes:

Supplementary Text

Methanol 6.7 GHz Flares in G33.64-0.21.

G33.64-0.21 is a high-mass star-forming region located at a kinematic distance of 4.0 kpc with an estimated infrared luminosity of $1.2\times10^4 L_\odot$ (*26*). The spectra of the 6.7 GHz methanol masers in G33.64-0.21 were monitored daily with the Yamaguchi 32-m Radio Telescope over several time intervals from 2009 to 2015 by Fujisawa *et al.* (*27*). The corresponding observations identified five narrow maser spectral features (Components I to V, defined with increasing line-of-sight velocity; see Fig. 1 of Fujisawa *et al.* (*27*)) with line widths of approximately $0.3\ \mathrm{km\,s^{-1}}$. Two bursts of radiation, lasting on the order of ten days, were observed in Component II ($v_{\mathrm{lsr}} = 59.6\ \mathrm{km\,s^{-1}}$) in July and August 2009, while all other velocity components did not exhibit any significant change in their flux densities over similar time-scales or longer (see Fig. 2 of Fujisawa *et al.* (*27*)). During both events, the flux densities increased approximately sevenfold within 24 hours and then returned to their original value while exhibiting a damped oscillator behavior. Subsequent observations with the Japanese VLBI Network revealed that Component II, responsible for the two bursts, emanates from the southwestern edge of G33.64-0.21 within a region measured to be much smaller than 70 AU. Different scenarios were proposed to explain these observations, but none were so far able to adequately describe an energy release mechanism responsible for such bursting behavior.

Given the damped oscillator character of the intensity curve during the bursts, we investigated the possibility of superradiance in the 6.7 GHz methanol line in an attempt to explain the energy relaxation mechanism at play for G33.64-0.21. Here, we focus on the second burst appearing in August 2009 in Fig. 2 of Fujisawa *et al.* (*27*). The results of our analyses show that a group of methanol superradiance large-samples of mean inverted column density $\langle nL\rangle \sim 7\times10^4\ \mathrm{cm^{-2}}$ (e.g., of density $\langle n\rangle \sim 0.1\,\mathrm{cm^{-3}}$ and length $\langle L\rangle \sim 10^6\ \mathrm{cm}$) can reproduce similar intensity variations as that of the 6.7 GHz line detected in G33.64-0.21. In figure S1 we show the average intensity (scaled to the data) obtained with 1000 such superradiance large-samples calculated using our one-

dimensional model (solid blue curve) superposed on the data from Fujisawa *et al.* (*27*) (black dots). The superradiance sample realizations are generated using $\langle T_{\mathrm{R}} \rangle = 1.1\,\mathrm{hr}$, $\sigma_{T_{\mathrm{R}}} = 0.07\langle T_{\mathrm{R}} \rangle$ and $T \leq 600\langle T_{\mathrm{R}} \rangle$. As seen in the figure, our superradiance model agrees well with the data and is successful in reproducing the main characteristics of the observed intensity curve.

The observations of Fujisawa *et al.* (*27*) were initially carried out daily (from Day 5039 to Day 5043 in fig. S1) followed by alternate day monitoring of the source. As a result, the data are sparse considering the rapid intensity variations exhibited by the superradiance curve. This also implies that the peak flux density detected by Fujisawa et al. (*27*) may not represent the actual maximum experienced by the source; our model indicates a peak flux density of 350 Jy late on Day 5042. Finally, the dephasing time-scale T' used to produce the solid curve is on the order of a month, which is reasonable within the expected gas densities $10^4\,\mathrm{cm}^{-3} < n_{\mathrm{H}_2} < 10^9\,\mathrm{cm}^{-3}$ and temperature $T < 300\,\mathrm{K}$ in G33.64-0.21 (*28*).

Water 22 GHz Flares in Cepheus A

Cepheus A (Cep A) with 14 compact HII regions is a high-mass star-forming site located at a distance of ~ 0.7 kpc (*7*). In 1978, the 22-GHz water observations toward this source revealed significant time variability to be followed by a strong burst at $v_{\mathrm{lsr}} = -8\,\mathrm{km\,s}^{-1}$ between April and December 1980. In October 1980, when this burst was in its decay phase Mattila *et al.* (*7*) started a three-year monitoring program of Cep A using the 14-m radio telescope of the Metsähovi Radio Research Station. This source was monitored through monthly observations until October 1983, except for a few time-spans where observations were repeated daily or every few days. In April 1983, the flux density of the water 22-GHz line at $v_{\mathrm{lsr}} = -11.2\,\mathrm{km\,s}^{-1}$ increased six fold over 10 days reaching its maximum value of 1700 Jy on April 18. Later on, over the following 40 days, the flux density decayed to a background value while exhibiting a damped oscillator behavior. During this phase, a few secondary maxima were detected every 15 days or so. Different

models were used to reproduce the observed light curve for this burst, but they were either unsuccessful in replicating the time-scale of the event or did not capture the secondary maxima.

In fig. S2 we show a superradiance intensity curve (scaled to the data) calculated using an ensemble of 1000 superradiance large-samples (solid blue curve) superposed on data from Fig. 4c of Mattila *et al.* (*7*) (black dots). The superradiance realizations are produced using $\langle T_{\rm R} \rangle = 8.2\,{\rm hr}$, $\sigma_{T_{\rm R}} = 0.1\langle T_{\rm R} \rangle$ and $T \¢= 700\langle T_{\rm R} \rangle$. As seen in the figure the superradiance curve (solid curve) occurs over similar time-scale as that for the data and analogously exhibits a peak followed by secondary maxima as it damps. The relative intensities of the secondary maxima match those of the data reasonably well while the main peak exceeds the data. Given the simplicity of our superradiance model we can conclude that the overall behaviour of the burst is well captured by this model.

It must be noted that the water rotational energy levels ($J_{\rm K_aK_c} = 6_{16}$ and 5_{23}) corresponding to the 22-GHz line are degenerate and, in principle, superradiance can simultaneously operate in more than one of the corresponding hyperfine components. This can complicate the line flux density analysis due to the variation of the relative intensity of the degenerate transitions and their time of occurrence, which our superradiance model does not account for since it employs a two-level system approximation. This may be partly responsible for the disagreement between the model's peak intensity and the data. Another factor that may have an impact is the large half-power beam width ($\approx 4'$) of the telescope used for these observations, which were inevitably sensitive to an extended region and perhaps suffer contamination from a number of sources.

Once again, the results of our analysis suggest that a large group of water superradiance samples of mean inverted column density $\langle nL \rangle \sim 6\times10^{4}\,{\rm cm}^{-2}$ (e.g., $\langle n \rangle \sim 1\,{\rm cm}^{-3}$ and $\langle L \rangle \sim 10^{5}\,{\rm cm}$) must be responsible for the observed radiation intensity. We also note that the dephasing time-scale $T \¢= 700\langle T_{\rm R} \rangle$ or 238 days resulting from our calculations is less restrictive than the estimated collision time-scales for a given molecular hydrogen density

$n_{H_2} = 10^8$ cm^{-3} at $T \sim 100$ K to ~ 200 K consistent with the pumping model of water masers (*20, 29*).

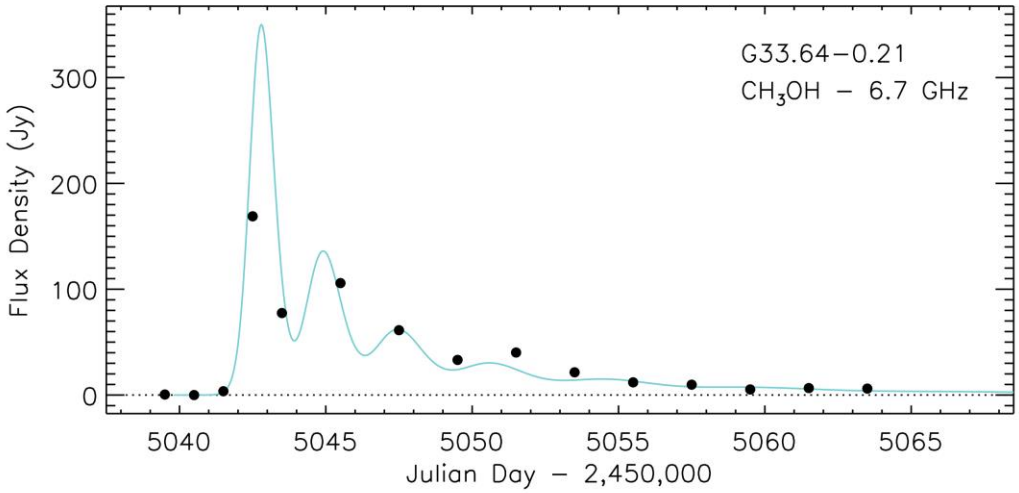

fig. S1. A superradiance large-sample intensity model (solid blue curve) superposed on the data from Fujisawa *et al.* (*27*) (black dots) obtained in July and August 2009 for the second 6.7-GHz methanol burst in G33.64-0.21. The superradiance intensity is averaged over 1000 large-samples taken from a Gaussian-distributed ensemble of T_R values of mean and standard deviation of $\langle T_R \rangle = 1.1$ hr and $\sigma_{T_R} = 0.07 \langle T_R \rangle$, respectively, and scaled to the data. The dephasing time scale was set to $T_2 = 600 \langle T_R \rangle$ for all samples, and the superradiance pulses were initiated from internal fluctuations characterized by an initial Bloch angle $\langle \theta_0 \rangle \sim 10^{-6}$ rad.

The data presented in fig. S1 (black dots) from Fujisawa et al. (27) obtained in July and August 2009 for the second 6.7-GHz methanol burst in G33.64-0.21. The first column is time in modified julian day and the second column is flux density in Jy where a background flux density of 22.4 Jy is subtracted from the data.

Time (Modified Julian Day)	Flux Density (Jy)
2455039.5	0.5
2455040.5	0
2455041.5	3.6
2455042.5	168.9
2455043.5	77.5
2455045.5	105.8
2455047.5	61.3
2455049.5	33.2
2455051.5	40.2
2455053.5	21.5
2455055.5	12
2455057.5	9.8
2455059.5	5.3
2455061.5	6.6
2455063.5	6.1

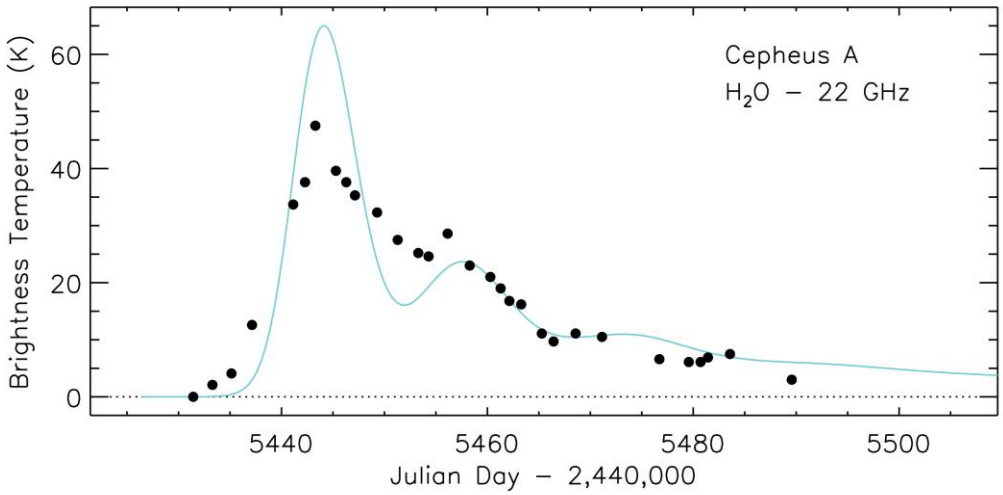

fig. S2. A superradiance large-sample intensity model (solid blue curve) superposed on the data from Mattila *et al.* (*7*) (black dots) obtained in April and May 1983 for the 22-GHz water burst at $v_{\rm lsr} = -11.2\,{\rm km\,s^{-1}}$ in Cepheus A. The superradiance intensity is generated using 1000 superradiance realizations with $\langle T_{\rm R} \rangle = 8.2\,{\rm hr}$, $\sigma_{T_{\rm R}} = 0.1\langle T_{\rm R} \rangle$, and a dephasing time-scale $T_2 = 700\langle T_{\rm R} \rangle$.

The data presented in fig. S2 (black dots) from Mattila et al. (7) obtained in April and May 1983 for the 22-GHz water burst $v_{lsr} = -11.2$ km s^{-1} in Cepheus A. The first column is time in modified julian day and the second column is the antenna temperature in units of Kelvin (K) after subtracting a backround value of 10 (K).

Time (Modified Julian Day)	T_A (K)
5431.43	0
5433.29	2.1
5435.14	4.1
5437.14	12.6
5441.14	33.7
5442.29	37.6
5443.29	47.5
5445.29	39.6
5446.29	37.6
5447.14	35.3
5449.29	32.3
5451.29	27.5
5453.29	25.2
5454.29	24.6
5456.14	28.6
5458.29	23
5460.29	21
5461.29	19
5462.14	16.8
5463.29	16.2
5465.29	11.1
5466.43	9.7
5468.57	11.1
5471.14	10.5
5476.71	6.6
5479.57	6.1
5480.71	6.1
5481.43	6.9
5483.57	7.5
5489.57	3

The data presented in Fig. 1 for the G107.298+5.639, illustrating the burst for the v_{lsr} = 8.57 kms^{-1} 6.7-GHz methanol (red dots) between modified julian day (MJD) 57,260 and 57,300 taken from Szymczak et al. 2016 (20). The first column is time in modified julian day and the second column is the flux density in units of Jansky (Jy).

Time (Modified Julian Day)	Flux Density (Jy)
57260.0488	0.05
57261.1943	-0.04
57261.7158	0.05
57262.8882	-0.30
57263.7563	0.59
57265.3413	0.51
57266.2988	2.25
57265.6792	0.40
57266.5366	4.15
57266.6611	5.13
57266.897	4.22
57267.0073	5.87
57267.0928	6.63
57267.2568	6.86
57267.3535	7.47
57267.6592	7.38
57267.8179	7.58
57267.9365	7.39
57268.04	7.19
57268.2163	7.34
57268.375	8.31
57268.4561	8.27
57268.5371	8.55
57268.6416	8.85
57268.7725	8.31
57268.8613	7.52
57268.9565	8.75
57269.1016	8.58
57269.272	10.03
57269.4688	9.64
57269.5942	11.45
57269.73	10.19
57269.7974	11.04
57269.8774	7.03
57269.978	9.33
57270.228	7.59

57270.373	7.42
57270.4585	6.03
57270.5571	5.32
57270.7549	4.85
57271.0752	4.46
57271.3789	4.53
57271.4893	4.16
57271.7974	3.89
57271.8755	2.86
57272.0225	2.30
57272.231	2.62
57272.5381	2.04
57272.7012	1.66
57272.8442	1.63
57272.9653	1.65
57273.2632	0.97
57273.8208	0.45
57273.9775	0.38
57274.1499	0.37
57274.3276	0.44
57274.6641	0.32
57274.5122	-0.02
57278.0913	0.06
57282.1807	0.02
57282.5767	-0.12
57284.8184	0.21
57286.0566	-0.12
57288.0674	-0.32
57290.2412	-0.22
57290.5039	-0.12
57291.6343	-0.04
57292.6865	-0.05
57295.1758	-0.14
57296.6772	-0.24
57297.2051	-0.27
57298.4595	0.27
57299.2319	-0.13
57299.6421	0.39

The data presented in Fig. 1 for the G107.298+5.639, illustrating the burst for v_{lsr} = 7.86 kms^{-1} 22-GHz water (blue dots in the figure). This data is taken from Szymczak et al. 2016 (20). The first column is time in modified julian day and the second column is the antenna temperature in units of Kelvin.

Time (Modified Julian Day)	T_A^*(K)
57273.9053	0.17
57275.2329	0.92
57276.29	1.33
57278.2603	2.22
57278.6138	2.36
57280.6768	4.59
57282.2676	3.70
57282.5024	5.43
57282.8013	4.87
57283.8535	4.83
57284.1772	5.39
57284.5601	7.34
57284.9487	5.12
57285.1152	5.66
57285.6597	6.14
57287.7104	5.77
57288.1152	6.22
57290.2056	5.89
57290.6162	5.10
57291.8076	3.96
57292.0005	3.86
57292.6118	4.92
57293.5229	5.27
57294.1265	3.65
57294.4839	4.08
57294.7793	3.03
57295.0444	3.63
57295.8618	3.18
57296.2183	2.55
57296.4902	3.78
57297.1812	2.17
57297.2256	2.36
57297.502	2.66
57298.4849	1.57
57298.4985	1.50
57299.6978	0.57
57303.1582	0.14